Microscopic features of moving traffic jams

Boris S. Kerner,[1,*] Sergey L. Klenov,[2,†] Andreas Hiller,[1,‡] and Hubert Rehborn[1,§]
[1]*DaimlerChrysler AG, REI/VF, HPC: G021, 71059 Sindelfingen, Germany*
[2]*Department of Physics, Moscow Institute of Physics and Technology, 141700 Dolgoprudny, Moscow Region, Russia*
(Received 12 July 2005; revised manuscript received 3 January 2006; published 7 April 2006)

Empirical and numerical microscopic features of moving traffic jams are presented. Based on a single vehicle data analysis, it is found that within wide moving jams, i.e., between the upstream and downstream jam fronts there is a complex microscopic spatiotemporal structure. This jam structure consists of alternations of regions in which traffic flow is interrupted and flow states of low speeds associated with "moving blanks" within the jam. Moving blanks within a wide moving jam resemble electron holes in the valence band of semiconductors: As the moving blanks that propagate upstream appear due to downstream vehicle motion within the jam, so appearance of electron holes moving with the electric field results from electron motion against the electric field in the valence band of semiconductors. Empirical features of moving blanks are found. Based on microscopic models in the context of the Kerner's three-phase traffic theory, physical reasons for moving blanks emergence within wide moving jams are disclosed. Microscopic nonlinear effects of moving jam emergence, propagation, and dissolution as well as a diverse variety of hysteresis effects in freeway traffic associated with phase transitions and congested traffic propagation are numerically investigated. Microscopic structure of moving jam fronts is numerically studied and compared with empirical results.

DOI: 10.1103/PhysRevE.73.046107 PACS number(s): 89.40.−a, 47.54.−r, 64.60.Cn, 05.65.+b

I. INTRODUCTION

Freeway traffic flow dynamics is one of the rapid developing fields of statistical and nonlinear physics (see the book [1], the reviews [2–8], and the conference proceedings [9–12]). Complexity of the physics of traffic is associated with diverse spatiotemporal traffic pattern features observed in real traffic [1]. It turns out that many of these features are qualitatively similar to those observed in other nonlinear nonequilibrium physical, biological, and chemical systems like electron-hole semiconductor plasma, composite superconductors, gas plasma, optical media, a nerve fiber, a cardiac muscle, chemical reactions, etc. (see, e.g., [13,14]). For this reason, a deep understanding of the physics of phase transitions and congested traffic patterns seems to be important for future development of general concepts and methods of the statistical and nonlinear physics.

In empirical freeway traffic observations, it has been found that traffic can be either free or congested. In congested traffic, a so-called "stop-and-go" phenomenon can be observed, i.e., a sequence of moving jams can appear (see the classic papers by Edie and Foote, Treiterer *et al.*, and Koshi *et al.* [15–20]). A moving jam is a localized structure propagating upstream. The jam is spatially restricted by two jam fronts in which the speed, density, and flow rate vary sharply. Within the upstream jam front, vehicles must decelerate to the speed in the jam. Within the downstream jam front, vehicles accelerate escaping from the jam.

Recently, from spatiotemporal analysis of empirical data measured over many days and years on various freeways in different countries, Kerner found that there are two different phases in congested traffic, synchronized flow and wide moving jam [1]. Thus there are three traffic phases: (1) free flow; (2) synchronized flow; and (3) wide moving jam. The fundamental difference between synchronized flow and wide moving jam is determined by the following macroscopic spatiotemporal objective (empirical) criteria, which define the synchronized flow and wide moving jam traffic phases in congested traffic [1]. The wide moving jam is a moving jam that exhibits the *characteristic, i.e., unique and coherent feature* to maintain the mean velocity of the downstream jam front, even when the jam propagates through any other traffic states or freeway bottlenecks. In contrast, synchronized flow does not exhibit this characteristic feature, in particular, the downstream front of synchronized flow is often *fixed* at a freeway bottleneck.

Earlier traffic flow models and theories reviewed in [2–8] explain the "stop-and-go" phenomenon as an instability of free flow against spontaneous moving jam emergence. Nonlinear analysis of this moving jam emergence from an initial free flow was firstly made in 1994 [21] for a homogeneous road and later for a road with an on-ramp bottleneck [22–25]. This theoretical analysis has revealed nonlinear features of moving jam emergence in the free flow, subsequent moving jam propagation, as well as diagrams of various types of "stop-and-go" phenomena occurring when flow rate changes on the homogeneous road [21,22] and at the bottleneck [23]. The main feature of this theory is that at a great enough flow rate the onset of congestion is associated with *spontaneous moving jam emergence in free flow*. Earlier traffic flow theories and models exhibit this fundamental feature both for a homogeneous road [21] and for bottlenecks [22–25] (see the review by Helbing [5] for a more detailed discussion).

However, recent empirical investigations of phase transitions and spatiotemporal congested patterns have shown that

*Electronic address: boris.kerner@daimlerchrysler.com
†Electronic address: s-klenov@mtu-net.ru
‡Electronic address: andreas.h.hiller@daimlerchrysler.com
§Electronic address: hubert.rehborn@daimlerchrysler.com

spontaneous moving jam emergence in free flow is *not* observed in real freeway traffic [26–28]. Rather than spontaneous moving jam emergence in free flow at an on-ramp bottleneck, in real traffic the onset of congestion (breakdown phenomenon) is associated with a first-order phase transition from free flow to synchronized flow ($F \rightarrow S$ transition); moving jams can emerge spontaneously later in this synchronized flow *only* ($S \rightarrow J$ transition) [26,27]. This empirical conclusion about the nature of the onset of congestion in real freeway traffic has been justified through numerous studies of breakdown phenomena in free flow at bottlenecks based on data, which have been measured over many days and years on different freeways in various countries; see a review of these empirical studies in Sec. 2.4 and part II of the book [1]. These *empirical* results that (i) the onset of congestion in free flow is associated with the $F \rightarrow S$ transition and (ii) moving jams emerge spontaneously only in synchronized flow contradict with the above-mentioned fundamental feature of earlier traffic flow theories and models reviewed and developed in [2–7,22–25].

For this reason, Kerner introduced a three-phase traffic theory, in which phase transitions between the free flow, synchronized flow, and wide moving jam traffic phases should explain complexity and nonlinear features of freeway traffic. The first microscopic models in the context of three-phase traffic theory introduced in 2002 are stochastic models [29,30]. Recently, deterministic three-phase traffic flow models have been developed [31]. As in empirical observations [26,27], in these models wide moving jams emerge spontaneously only in synchronized flow, i.e., the models exhibit the sequence of $F \rightarrow S \rightarrow J$ transitions leading to wide moving jam emergence in free flow; in addition, the models show all types of congested patterns found in empirical observations [1,29–33].

Nevertheless, microscopic features of moving jams have not been understood sufficiently up to now. Based on a single vehicle data analysis, we find in this paper that within wide moving jams there is a complex microscopic spatiotemporal structure. This jam structure consists of alternations of regions in which traffic flow is interrupted and flow states of low speeds associated with "moving blanks" within the jam. Note that wide moving jam propagation through a freeway bottleneck is associated with traffic flow interruption within the jam: Vehicles are stopped within the jam during a time interval, which is considerably longer than the mean time delay in vehicle acceleration at the downstream jam front. Thus flow interruption within wide moving jams can be used as a microscopic criterion for distinguishing between the wide moving jam and synchronized flow phases in congested traffic, even if single vehicle data is measured at a single freeway location [34].

In this paper, based on an empirical single vehicle data analysis microscopic spatiotemporal structure of moving jams and their microscopic features are found. These empirical features have been explained using numerical simulations of a stochastic microscopic model in the context of three-phase traffic theory. The paper is organized as follows. Empirical and theoretical features of moving blanks within wide moving jams are considered in Secs. II and III, respectively. In Sec. IV, microscopic features of the jam fronts, jam emergence, propagation, and dissolution as well as the associated hysteresis effects in traffic are numerically studied.

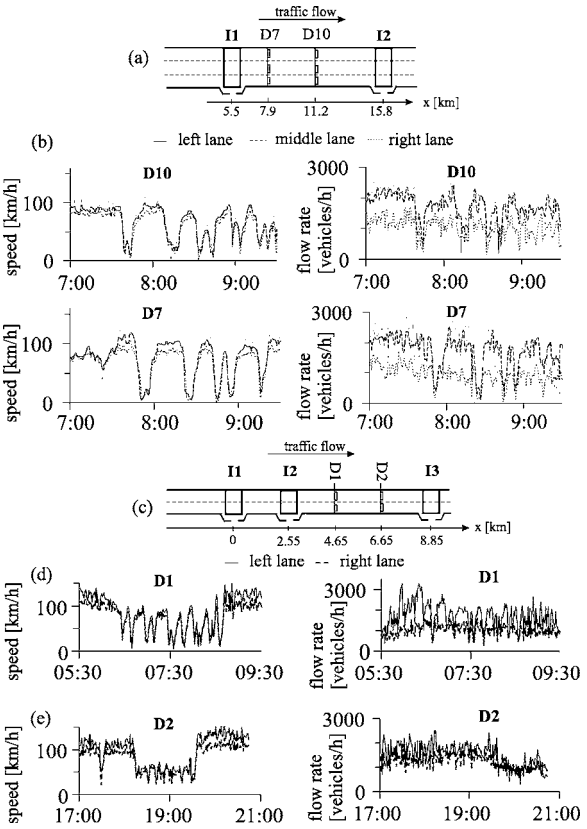

FIG. 1. Empirical macroscopic characteristics of single vehicle data measured on the freeway A5-South [(a) and (b)] and on the freeway A92-West [(c)–(e)]: (a) Sketch of detector arrangement of a section on the freeway A5-South. (b) Local traffic dynamics (1-min average data) of the speed (left) and flow rate (right) in three freeway lanes on December 12, 1995. (c) Sketch of detector arrangement on a section of the freeway A92-West. (d) and (e) Local traffic dynamics (1-min average data) of the speed (left) and flow rate (right) on July 17, 2000 (d) and August 23, 2000 (e) in both freeway lanes.

II. EMPIRICAL STUDY OF MOVING BLANKS WITHIN WIDE MOVING JAMS

A. Congested states in single vehicle data

Single vehicle characteristics are usually obtained either in driver experiments or through the use of detectors (e.g., [20,35–43]). In the latter case, data from a single freeway location or aggregated data measured at different locations are used [44].

Single vehicle data used in the paper have been measured on two different freeways in Germany. The first single vehicle data set has been measured on the three-lane freeway section of the freeway A5-South at detectors 10 and 7 [Fig. 1(a)]; a detailed consideration of this freeway section is made in [27]. For an overview of moving jams observed in single vehicle data, the data averaged over 1-min intervals is shown in Fig. 1(b). The second set of single vehicle data has

been measured on a two-lane section of the freeway A92-West at detectors D1 and D2 between intersections "AS Freising-Süd" (I2) and "AK Neufahrn" (I3) near Munich Airport [intersection I1: "AS Flughafen" in Fig. 1(c)] [45]. Local dynamics of the average speed and flow rate (1-min averaged data) for two typical days at which congested traffic have been observed are shown in Figs. 1(d) and 1(e).

In both freeway sections, single vehicle data is measured through the use of two sets of double induction loop detectors. A detector set consists of two detectors for each of the freeway lanes. A detector registers a vehicle by producing an electric pulse whose duration Δt_i is related to the time taken by the vehicle to traverse the induction loop. This enables us to calculate the gross time gap between two vehicles i and $i+1$ that have passed the loop one after the other $\tau_{i,i+1}^{(\mathrm{gross})}$. There are two detector loops in each detector. The distance between these loops is constant. This enables us to calculate the individual vehicle speed v_i and estimate the vehicle length $d_i = v_i \Delta t_i$ as well as the net time gap (time headway) between the vehicles i and $i+1$: $\tau_{i,i+1} = \tau_{i,i+1}^{(\mathrm{gross})} - \Delta t_i$.

B. Flow interruption effect within wide moving jams

Within wide moving jams, i.e., between the jam fronts, there are regions in which traffic flow is interrupted. A condition for flow interruption is [34]

$$\tau_{\max} \gg \tau_{\mathrm{del}}^{(\mathrm{ac})}, \tag{1}$$

where $\tau_{\max}$ is the maximum time headway between two vehicles within the jam and $\tau_{\mathrm{del}}^{(\mathrm{ac})}$ is the mean time delay in vehicle acceleration at the downstream jam front from a standstill within the jam. Under condition (1), there are at least several vehicles within the jam that are in a standstill or if they are still moving, it is only with a negligible low speed in comparison with the speed in the jam inflow and outflow. These vehicles separate vehicles accelerating at the downstream jam front from vehicles decelerating at the upstream jam front: The inflow into the jam has no influence on the jam outflow. Then the jam outflow is fully determined by vehicles accelerating at the downstream jam front. In an example, flow interruption effect occurs two times during jam propagation through detector D10 [46] [Figs. 2(a)–2(g); these time intervals are labeled "flow interruption" in Fig. 2(g)]. The values $\tau_{\max}$ for the first flow interruption intervals within the wide moving jam are equal to approximately 20 s in the left lane, 22 s in the middle line, and 30 s in the right line. These values $\tau_{\max}$ satisfy the criterion (1) because corresponding to empirical results $\tau_{\mathrm{del}}^{(\mathrm{ac})} \approx 1.5-2$ s [1].

It should be noted that traffic flow interruption intervals within the jam in different freeway lanes do not necessarily occur at the same time. Whereas the first flow interruption interval appears almost simultaneously in all freeway lanes, the second one occurs in the left lane earlier than in the middle and right lanes [Figs. 2(a)–2(g)]. In other empirical examples of wide moving jams, the flow interruption effect occurs in some of the freeway lanes only whereas in other lane(s) there is no flow interruption. It turns out that even in this case a moving jam can be a wide moving one, i.e., the jam propagates through a bottleneck while maintaining the

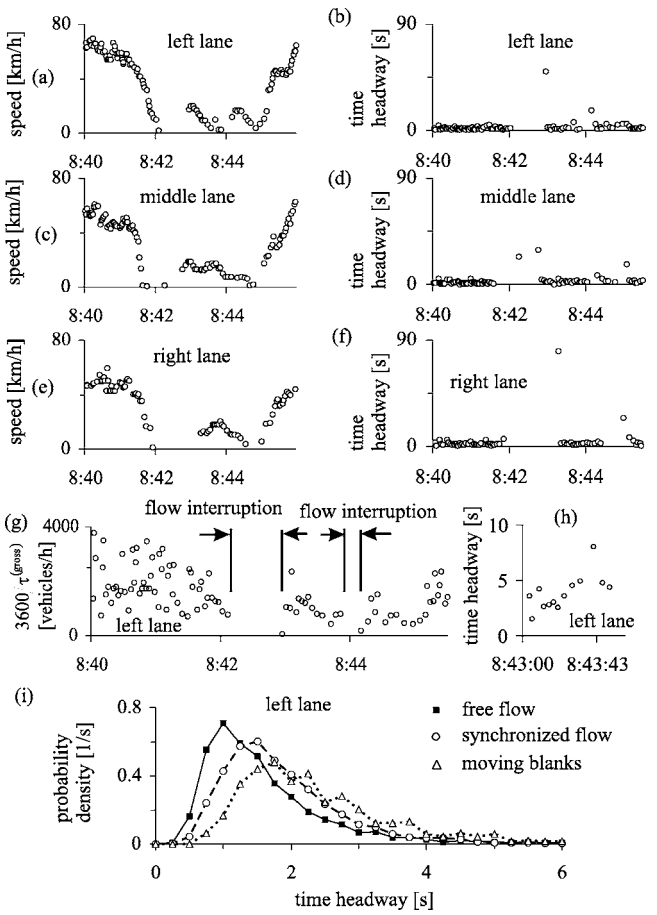

FIG. 2. Empirical microscopic structure of wide moving jams: (a)–(f) Single vehicle data for speed within a wide moving jam [(a), (c), and (e)] and the associated time headways [(b), (d), and (f)] in the left [(a) and (b)], middle [(c) and (d)], and right lanes [(e) and (f)] related to the example at D10 in Fig. 1(b). (g) Time distributions of the value $3600/\tau^{(\mathrm{gross})}$ in the left lane. (h) Time headways associated with moving blanks in the left lane related to the jam shown in (a). (i) Probability density of time headways in the left lane for free flow (solid curve), synchronized flow (dashed curve), and moving blanks within wide moving jams (dotted curve). In (i), an aggregated single vehicle data set is used [44], which is related to aggregation of the data sets measured on December 12, 1995, July 17, 2000, and August 23, 2000 shown in Figs. 1(b), 1(d), and 1(e); $\bar{\tau}_{\mathrm{free}} = 1.55$, $\bar{\tau}_{\mathrm{syn}} = 1.76$, and $\bar{\tau}_{\mathrm{blanks}} = 3.15$ s.

mean velocity of the downstream jam front, if the relation $\tau_{\max} / \tau_{\mathrm{del}}^{(\mathrm{ac})}$ for the lane(s) with flow interruption within the jam is great enough [34]. Similar results are found for other moving jams in single vehicle data, i.e., for the example measured on the freeway A92-West [Fig. 1(d)].

In another example shown in Fig. 1(e), there are also many moving jams during the time intervals of congested traffic. The speed within two moving jams in Fig. 3(a) is also very low. Nevertheless, rather than wide moving jams these moving jams should be classified as narrow moving jams [1,34]. This is because there are no traffic flow interruptions within these moving jams [Fig. 3(a)]. Indeed, upstream and downstream of the jams, as well as within the jams there are many vehicles that traverse the induction loop detector: There is no qualitative difference in time headways for dif-

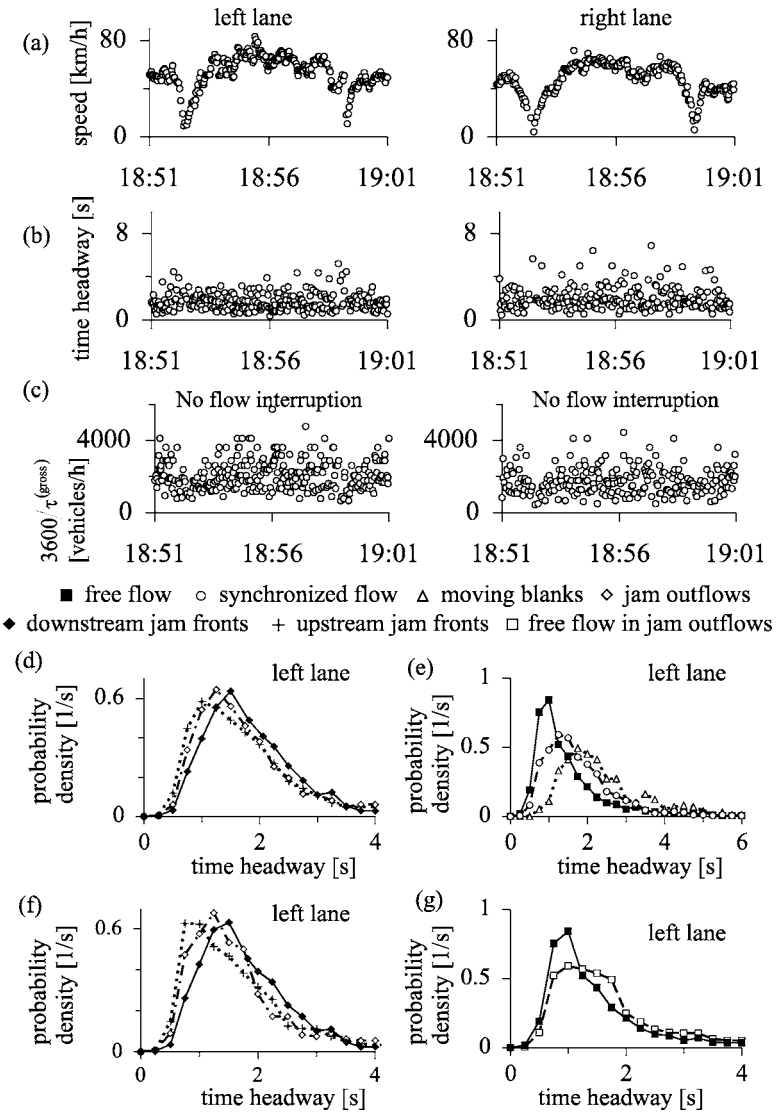

FIG. 3. Empirical microscopic structure of narrow moving jams [(a)–(c)] and empirical probability density of time headways in different traffic phases [(d)–(g)]: (a)–(c) Single vehicle data for speed within a sequence of two narrow moving jams in the left (left) and right lanes (right) (a) as well as the associated time distributions of time headways τ (b) and of the value $3600/\tau^{(\mathrm{gross})}$ (c) related to data shown in Fig. 1(e). (d) and (f) Probability density of time headways in the left lane for downstream jam fronts (solid curve), upstream jam fronts (dotted curve), and jam outflows (dashed-dotted curve): (d) for the same aggregated data as those in Fig. 2(i); (f) only for the data set shown in Fig. 1(d). In (d), $v_{\mathrm{max\,J}}^{(\mathrm{syn})}=19.8$ m/s, $\bar{d}=4.6$ m, $\bar{d}_{\mathrm{jam}}=6.9$ m, $\bar{\tau}_{\mathrm{up}}=1.62$ s, $\bar{\tau}_{\mathrm{out}}^{(\mathrm{syn})}=1.69$ s, and $\bar{\tau}_{\mathrm{down}}=1.77$ s. In (f), $v_{\mathrm{max\,J}}^{(\mathrm{syn})}=22.9$ m/s, $\bar{d}=4.5$ m, $\bar{d}_{\mathrm{jam}}=6.5$ m, $\bar{\tau}_{\mathrm{up}}=1.53$ s, $\bar{\tau}_{\mathrm{out}}^{(\mathrm{syn})}=1.56$ s, and $\bar{\tau}_{\mathrm{down}}=1.73$ s. (e) Probability density of time headways in the left lane for free flow (solid curve), synchronized flow (dashed curve), and moving blanks (dotted curve) for the data set shown in Fig. 1(d); $\bar{\tau}_{\mathrm{free}}=1.48$, $\bar{\tau}_{\mathrm{syn}}=1.67$, and $\bar{\tau}_{\mathrm{blanks}}=3.17$ s. (g) Probability density of time headways in the left lane for free flow (solid curve) taken from (e) and for free flow in jam outflows only (dashed curve) for the data set shown in Fig. 1(d).

ferent time intervals associated with these narrow moving jams and in traffic flow upstream or downstream of the jams [Figs. 3(b) and 3(c)]. This can be explained if it is assumed that each vehicle, which meets a narrow moving jam, must decelerate at the upstream jam front to a very low speed within the jam (sometimes as low as zero), can nevertheless accelerate at the downstream jam front almost without any time delay within the jam: The narrow moving jam consists of upstream and downstream jam fronts only. These assumptions are confirmed by single vehicle data shown in Figs. 3(b) and 3(c), in which time headways and the value $3600/\tau^{(\mathrm{gross})}$ for different vehicles exhibit the same behavior away and within the jams. Thus, regardless of these narrow moving jams traffic flow is not discontinuous: The narrow moving jams are associated with the synchronized flow phase [48].

Results of wide moving jam identification based on the macroscopic spatiotemporal empirical (objective) criteria, which define the synchronized flow and wide moving jam phases in congested traffic [1], and on the microscopic criterion (1) have been compared in [34]. This comparison allows us to suggest that the moving jam in Figs. 2(a)–2(f) for which the criterion (1) is satisfied is associated with the wide moving jam phase: The jam propagates through a bottleneck while maintaining the mean velocity of the downstream jam front. In contrast, narrow moving jams in Figs. 3(a)–3(c), for which the criterion (1) is not satisfied, are associated with the synchronized flow phase: Narrow moving jams are caught at the bottleneck [34]. This is because in contrast with wide moving jams, there is no flow interruption within the narrow moving jams.

C. Definition of moving blanks and their attributes

Between flow interruption intervals in Figs. 2(a)–2(g), vehicles within the jam exhibit time headways about 1.5–7 s [Fig. 2(h)]. These time headways are considerably shorter than flow interruption intervals (about 20 s and longer) in Figs. 2(b) and 2(g) discussed above. The time headways are related to low speed states measured at detectors within the jam [Figs. 2(a), 2(c), and 2(e)].

To understand effect of these low speed states, note that when vehicles meet the wide moving jam, first they decelerate at the upstream jam front to a standstill. As a result, the

first flow interruption interval in all lanes appears [Figs. 2(a)–2(g)]. Net distances (space gaps) between these vehicles can be very different and the mean space gap can exceed a minimum (safe) space gap considerably, i.e., regions with no vehicles can appear within the jam. These regions with no vehicles are called *blanks* within the wide moving jam.

Later vehicles move covering these blanks. This low speed vehicle motion is responsible for low speed states mentioned above [Figs. 2(a), 2(c), and 2(e)]. Consequently, due to this vehicle motion new blanks between vehicles occur upstream, i.e., the blanks move upstream within the jam. Then other vehicles within the jam that are upstream of these blanks also begin to move covering the latter blanks. This leads to moving blanks that propagate upstream within the jam.

Thus we define a *moving blank* as a blank between vehicles, which moves upstream due to vehicle motion within the jam. The vehicle motion occurs at a low vehicle speed, i.e., the vehicle motion creating moving blanks within the jam is related to low speed states discussed above [Figs. 2(a), 2(c), and 2(e)]: these low speed states are the reason of moving blank emergence within the jam. This explains why moving blanks are associated with low speed states within the jam.

Time headways τ between vehicles in these low speed states with moving blanks are about 1.5–7 s [Figs. 2(h) and 2(i)]. Because these low speed states are the reason for moving blanks, we will refer the time headways in the low speed states to moving blanks. Thus the term *time headways for moving blanks* used below means the time headways in the low speed states causing upstream motion of blanks.

To explain possible short time headways associated with moving blanks observed in empirical data (about 1.5 s), note that when vehicles begin to cover a blank within a wide moving jam, they start to move from a standstill within the jam. Thus some of the vehicles can move with time headways between each other that are close to a time delay in vehicle acceleration from a standstill within the jam whose average value is $\tau_{\mathrm{del}}^{(\mathrm{ac})} \approx 1.5-2$ s.

Time headways in low speed states within the jam, i.e., time headways associated with moving blanks [about 1.5–7 s in Figs. 2(h) and 2(i)] must be distinguished from long time intervals of traffic flow interruption within the jam (about 20 s and longer) found in empirical observations [Figs. 2(b), 2(d), and 2(f)]. The flow interruption intervals within the jam occur when some of the vehicles within the jam do not move at all. This vehicle stoppage does not indicate whether there are some blanks between these vehicles or not. This is because during these long flow interruption intervals space gaps between vehicles that are stopped within the jam might be quite small.

Thus, at a fixed freeway location, within a wide moving jam long time intervals, in which no vehicle passes the location (flow interruption intervals), alternate with time intervals in which vehicles pass the location with low speeds and time headways of about 1.5–7 s associated with moving blanks within the jam. This empirical result could be associated with the following microscopic jam space structure: freeway regions in which vehicles are in a standstill (traffic flow interruption) alternate with freeway regions in which blanks moving upstream (moving blanks) occur resulting from vehicle motion with low speeds.

Empirical data show that low speed states within wide moving jams associated with moving blanks are not necessarily synchronized between different lanes [Figs. 2(a), 2(c), and 2(e)].

Moving blanks within a wide moving jam resemble electron holes in the valence band of semiconductors: As the moving blanks that propagate upstream appear due to downstream vehicle motion within the jam, so appearance of electron holes moving with the electric field results from electron motion against the electric field in the valence band of semiconductors. However, an electron hole is associated with a single vacancy for one electron in the valence band. In contrast, there can be wide (in the longitudinal direction) moving blanks associated with a "vacancy" for two or more vehicles within a wide moving jam. This moving blank can be split into two or more moving blanks during upstream blanks motion. On the other hand, several adjacent moving blanks can merge into one moving blank.

D. Time headway distributions in traffic phases

The time headway $\tau_{\mathrm{blanks}}^{(\mathrm{m})}$, at which probability density of time headways for moving blanks has the maximum point, is longer than the one $\tau_{\mathrm{syn}}^{(\mathrm{m})}$ for synchronized flow. The latter is longer than the associated time headway $\tau_{\mathrm{free}}^{(\mathrm{m})}$ for free flow [Fig. 2 (i)]; the same conclusions can be made for the associated mean time headways, respectively,

$$\overline{\tau}_{\mathrm{blanks}} > \overline{\tau}_{\mathrm{syn}} > \overline{\tau}_{\mathrm{free}}. \tag{2}$$

In addition, for τ longer than $\tau_{\mathrm{blanks}}^{(\mathrm{m})}$ probability density of τ associated with moving blanks is a considerably weaker decreasing function of τ than this is the case for τ longer than $\tau_{\mathrm{syn}}^{(\mathrm{m})}$ and $\tau_{\mathrm{free}}^{(\mathrm{m})}$ for probability densities of τ associated with synchronized flow and free flow, respectively. This is explained by longer τ (3–7 s), which are often observed in moving blanks.

If time headways for downstream jam fronts, jam outflows, and upstream jam fronts are analyzed separately, we find the following empirical results: (i) The time headway $\tau_{\mathrm{down}}^{(\mathrm{m})}$, at which probability density of τ for downstream jam fronts [solid curve in Fig. 3(d)] has the maximum point, is longer than the one $\tau_{\mathrm{out}}^{(\mathrm{syn,m})}$ for synchronized flow in jam outflows (dashed-dotted curve). The latter is longer than the associated time headway $\tau_{\mathrm{up}}^{(\mathrm{m})}$ for upstream jam fronts (dotted curve). The same conclusions can be made for the associated mean time headways, respectively;

$$\overline{\tau}_{\mathrm{down}} > \overline{\tau}_{\mathrm{out}}^{(\mathrm{syn})} \gtrsim \overline{\tau}_{\mathrm{up}}. \tag{3}$$

(ii) Data related to downstream jam fronts and jam outflows have the most influence on the time headway distribution in synchronized flow. (iii) Jam outflows are responsible for relatively long values $\tau_{\mathrm{free}}^{(\mathrm{m})}$ and $\overline{\tau}_{\mathrm{free}}$ for free flow [Fig. 2 (i)] in comparison with appreciably shorter time headways $\tau_{\mathrm{free}}^{(\mathrm{m})}$ and $\overline{\tau}_{\mathrm{free}}$ found earlier in other data for free flow (e.g., [35,36,41]). (iv) For the mean time headway $\overline{\tau}_{\mathrm{out}}^{(\mathrm{syn})}$ in jam outflows, the following condition is approximately satisfied (with a small error that is less than 2%) [49]

$$\bar{\tau}_{\text{out}}^{(\text{syn})} = \tau_{\text{del}}^{(\text{ac})} + \bar{g}_{\text{jam}}/v_{\text{max J}}^{(\text{syn})}. \quad (4)$$

In Eq. (4), $\bar{g}_{\text{jam}}=\bar{d}_{\text{jam}}-\bar{d}$ is the mean space gap between vehicles stopped within wide moving jams, $\bar{d}_{\text{jam}}=1/\rho_{\max}$, $\rho_{\max}$ is the jam density, $\bar{d}$ is the mean vehicle length; $v_{\text{max J}}^{(\text{syn})}$ is the mean speed in jam outflows, $v_{\text{max J}}^{(\text{syn})}=q_{\text{out}}^{(\text{syn})}/\rho_{\text{min J}}^{(\text{syn})}$, $q_{\text{out}}^{(\text{syn})}$ is the jam outflow rate, and $\rho_{\text{min J}}^{(\text{syn})}$ is the mean density in jam outflows. An explanation of Eq. (4) appears in the Appendix.

Qualitatively the same results are found for each of the data sets in Figs. 1(b), 1(d), and 1(e), as shown for one of these data sets in Figs. 3(e) and 3(f). In particular, an explanation of item (iii) is illustrated in Fig. 3(g): Probability density of τ for free flow in jam outflows (dashed curve) is markedly shifted to longer time headways in comparison with the one for all data in free flow (solid curve).

E. Empirical characteristics of traffic phases in flow-density and speed-density planes

A comparison of average characteristics of low vehicle speeds within a wide moving jam associated with moving blanks (cross and triangle points) with free flow (black squares), synchronized flow (circles), and the line *J* for the downstream jam front (line *J*) is presented in the flow-density and speed-density planes (Fig. 4). Here, a moving averaging of five vehicles passing the detector has been performed. As found earlier [35–37] (see Fig. 1 in [37]), very small density states associated with low vehicle speeds are observed within wide moving jams [crosses in Figs. 4(a) and 4(b)]. Due to these "characteristic" small density states within wide moving jams [crosses in Figs. 4(a) and 4(b)] the flow rate is usually on average an increasing function of density in the flow-density plane [cross plus triangle points in Fig. 4(a)].

However, a single vehicle analysis of these small density points that has been made allows us to conclude [47] that these points [crosses in Fig. 4(a)] as well as the related increasing function of the flow rate with density associated with wide moving jams [37] result from a *large systematic error*. This error is associated with incorrect density estimation within the jams made in Refs. [35–37].

To understand this critical conclusion about microscopic empirical study of traffic phases made in Refs. [35–37], recall that there are traffic flow interruption intervals within the wide moving jam [Figs. 2(b), 2(d), and 2(f)]. This leads to an incorrect calculation of the average speed v within the jam. The average speed measured by a detector can be related to a time interval, which includes at least one traffic flow interruption interval. In this case, the measured average speed is considerably higher than the real average speed within the jam. This is because vehicles do not move during traffic flow interruption intervals. As a result, the subsequent density estimation through the formula $\rho=q/v$ (q the flow rate) leads to very small densities within the jam. However, the real density of vehicles stopped within the jam during traffic flow interruption is very large. Thus the single vehicle data associated with the traffic flow interruption effect within wide moving jams cannot be used for density estimation within

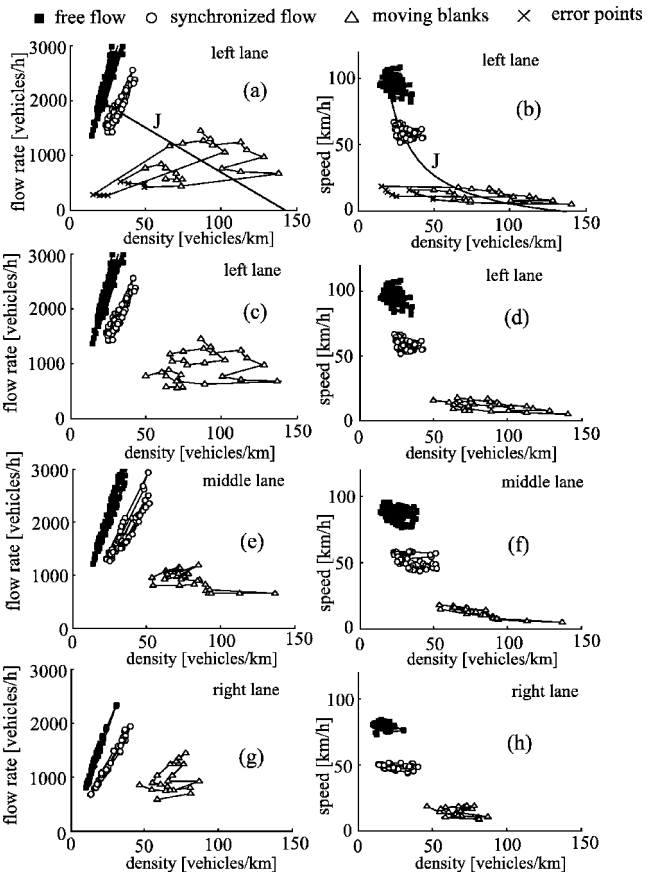

FIG. 4. Empirical characteristics of traffic phases: (a) and (b) Traffic phases in the flow-density (a) and speed-density (b) planes for data in the left lane together with the line *J* (a) and the curve *J* (b) associated with propagation of the downstream front of the wide moving jam (the physics of the line *J* see in [1]). (c)–(h) Traffic phases in the flow-density [(c), (e), and (g)] and speed-density [(d), (f), and (h)] planes in the left [(c) and (d)], middle [(e) and (f)], and right [(g) and (h)] lanes when *improved data* for moving blanks are only considered. Moving averaging over five vehicles is used. Data is related to the example at D10 in Fig. 1(b) .

the jams. To estimate real vehicle density within a wide moving jam during time intervals that include flow interruption intervals, the density definition (number of vehicles per freeway length at a given time moment), i.e., *spatial averaging*, should be used, rather than density estimation through the use of the formula $\rho=q/v$ in which the flow rate and average speed are related to *time averaging* of vehicles passing a detector during a given time interval. The spatial averaging (density definition) is not possible to apply when data is measured at detectors whose locations are far away from each other [Figs. 1(a) and 1(c)]. The conclusion about the large systematic error in density estimation within wide moving jams is confirmed by a numerical analysis made in Sec. III.

This analysis shows also that within wide moving jams density estimation $\rho=q/v$ exhibits a relatively small error during non-interrupted vehicle motion associated with moving blanks within the jams. This is because in this case the associated time headways are related to vehicles moving within the jams. If only these single vehicle data are used for

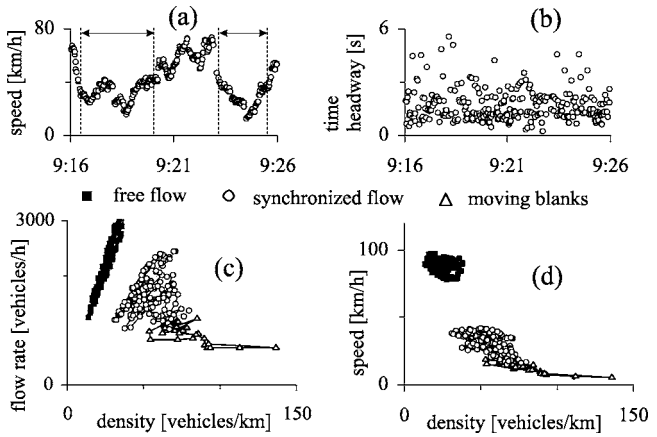

FIG. 5. Empirical characteristics of traffic phases: (a) and (b) Single vehicle data for speed (a) and time headways (b) for synchronized flow at D10 related to Fig. 1(b). (c) and (d) Traffic states averaged over five vehicles (moving average) associated with synchronized flow in (a) and with moving blanks within the jam taken from Figs. 4(e) and 4(f) in the flow-density (c) and speed-density planes (d). Arrows in (a) show time intervals of synchronized flow states used in (c) and (d). Middle freeway lane.

density estimation, then points for moving blanks within the jam appear that are associated with random transformations in different directions in the flow-density plane [triangle points in Figs. 4(c), 4(e), and 4(g)] rather than an increasing function of the flow rate with density [cross and triangle points in Fig. 4(a)]. This is explained by low vehicle speed states that are associated with nonregular vehicle motion covering blanks within the wide moving jam.

In Fig. 4, points for synchronized flow are related to the jam inflow. The speed in these states is considerably higher than the speed within low speed states associated with moving blanks within the jam. For this reason, three types of points (for free flow, synchronized flow, and moving blanks within the wide moving jams) appear that are separated one from another in the flow-density and speed-density planes. These separated traffic states for the three traffic phases—free flow, synchronized flow, and wide moving jams—are in accordance with states on theoretical double Z-characteristics of three-phase traffic theory (see Sec. 6.4 in [1] and numerical simulations in Sec. IV A below), if low speed states within the wide moving jam are taken into account.

However, synchronized flow states can overlap states associated with moving blanks within a wide moving jam (Fig. 5). This is because the speed in synchronized flow states can be as low as the speed in states associated with moving blanks within the jam. Thus, in a general case low speed states associated with moving blanks within wide moving jams cannot be used for clear distinguishing of the synchronized flow and wide moving jam phases in congested traffic.

III. NUMERICAL SIMULATIONS OF MOVING BLANKS

In numerical simulations presented below, we use stochastic microscopic models and model parameters of Refs. [32,33,52]. The main idea of these models is the speed adaptation effect in synchronized flow for a vehicle that cannot pass the preceding vehicle. Within a so-called "synchronization gap," the vehicle tends to the adjust its speed to preceding vehicle without caring what the precise space gap is, as long as it is safe. To simulate driver behavior in various traffic conditions, acceleration and deceleration delays depend on whether a vehicle currently decelerates or accelerates as well as on the vehicle speed.

A. Propagation of moving blanks within wide moving jam induced in heterogeneous free flow

To understand features of propagation and evolution of moving blanks within a wide moving jam, we consider a moving jam that is induced downstream of an on-ramp bottleneck by applying of a short-time and high amplitude local speed disturbance in heterogeneous free flow consisting of fast and long vehicles [Figs. 6(a) and 6(b)]. There are two time intervals in which flow interruption within the jam occurs. The maximum time headways [Fig. 6(c)] associated with these flow interruption effects satisfy the criterion (1) (model time delays for fast and long vehicles are $\tau_{\mathrm{del}}^{(\mathrm{ac})} \approx 1.77$ and 3.33 s, respectively) in the left and right freeway lanes. As a result, in accordance with the macroscopic spatiotemporal criteria for the wide moving jam phase, this jam propagates through the bottleneck while maintaining the mean velocity of the downstream jam front.

Within the wide moving jam, between time intervals of flow interruptions there are intervals in which low speed states appear associated with moving blanks [Figs. 6(b)–6(d)]. Simulated time headways for moving blanks that are about 2.5–7.5 s in the left lane [Fig. 6(d), left] [53] correspond to empirical observed values [Figs. 2(h) and 2(i)]. As can be seen from vehicle trajectories within the jam, these low speed states and associated moving blanks are related to nonhomogeneous vehicle motions that cover blanks between vehicles within the jam (Fig. 7). These moving blanks propagate upstream with a negative velocity that is on average equal to the characteristic speed of the downstream jam front. Spatial and temporal speed distributions in low speed states associated with moving blanks exhibit complex variations within the jam, which are different in the left and right lanes [Figs. 7(b) and 7(c)]; these variations seem to correspond to a random vehicle speed behavior within the jam.

Due to flow interruption within the wide moving jam shown in Figs. 6(a)–6(c), there is a large error in density distributions calculated through the formula $\rho = q/v$ at greater density [curves 2 in Fig. 6(e)] in comparison with density distributions found based on the density definition (vehicles per freeway length) (curves 1). Indeed, curves 2 in Fig. 6(e) show a significant density underestimation within moving jams. These error points [crosses in Fig. 8(a)] explain the systematic error in the empirical studies of states within wide moving jams made in Refs. [35–37] that has been illustrated in Figs. 4(a) and 4(b) [compare error points in Figs. 4(a), 4(b), and 8(a)].

Within the regions of moving blanks, the difference between density calculated through the formula $\rho = q/v$ [curves

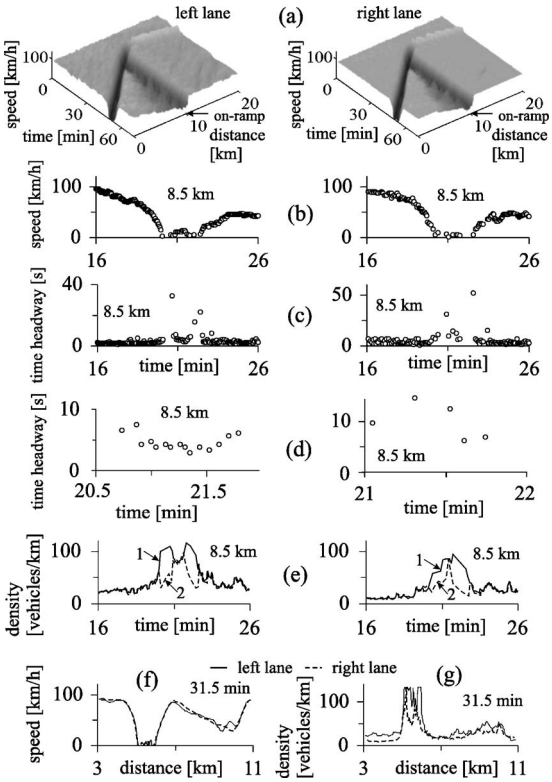

FIG. 6. Simulated characteristics of moving blanks within a wide moving jam propagating through an on-ramp bottleneck. (a) Speed in space and time on the main road. (b)–(e) Single vehicle data for time dependences of speed (b), time headways (c) and (d), and the associated density distributions calculated through the density definition (solid curves 1) and the formula $\rho=q/v$ (dashed curves 2) (e) at location $x=8.5$ km. Left and right figures (a)–(e) are related to the left and right lanes, respectively. In (e) for density calculation, a moving averaging over platoons of five vehicles is performed. To use the density definition for calculations of curves 1 in (e), at a time moment when one of the vehicles has just been detected at $x=8.5$ km the density within a vehicle platoon is calculated. This platoon consists of the detected vehicle and two vehicles upstream and two vehicles downstream. In contrast, calculations of curves 2 in (e) is performed as in empirical observations shown in Figs. 4(a) and 4(b), i.e., the flow rate q and average speed v measured by the detector are used in formula $\rho=q/v$. (f) and (g) Speed (f) and density (g) related to (a) as functions of distance at time 31.5 min in the left and right lanes. Model of heterogeneous traffic of Sec. 20.2 in [1] with 80% fast and 20% long vehicles; $\tau_{\mathrm{del}}^{(a,j)}(v)=\tau/p_0^{(j)}(v)$, $p_0^{(j)}(v)=[a^{(j)}+b^{(j)}\ \min(1,v/10)]$, $j=1,3$; $a^{(1)}=0.565$, $b^{(1)}=0.085$ for fast vehicles ($j=1$), and $a^{(3)}=0.3$, $b^{(3)}=0.18$ for long vehicles ($j=3$). $q_{\mathrm{in}}=1565$, $q_{\mathrm{on}}=337$ vehicles/h/lane. $q_{\mathrm{out}}=1900$ and 1100 vehicles/h in the left and right lanes, respectively. On-ramp location is $x_{\mathrm{on}}=10$ km, on-ramp merging region length is $L_{\mathrm{m}}=300$ m. The wide moving jam is excited by local perturbations applied during 3 min in both lanes at the location 1250 m downstream of the end of the on-ramp merging region.

2 in Fig. 6(e)] and density found based on the density definition (curves 1) decreases considerably. For this reason, if error points associated with flow interruption within the jam are removed, then remaining points in the flow-density [Fig.

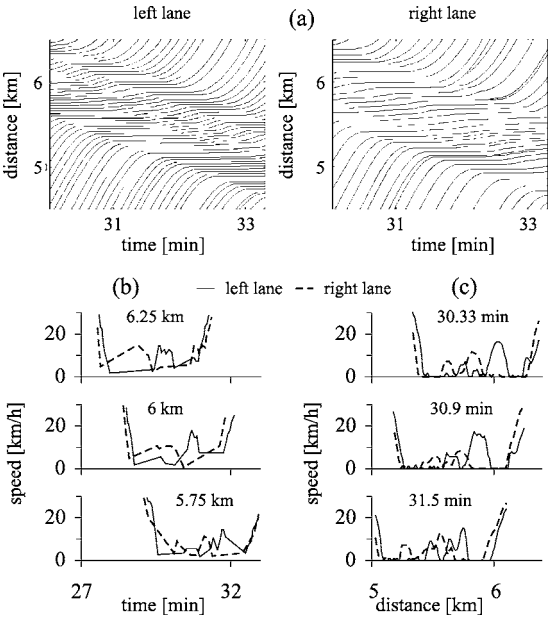

FIG. 7. Simulated microscopic characteristics of moving blanks within the wide moving jam shown in Fig. 6(a): (a) Vehicle trajectories for each fourth vehicle in the left (left) and right (right) lanes. (b) and (c) Low speed states associated with moving blanks at three different locations (b) and three different time moments (c) in the left and right lanes.

8(b)] and speed-density planes [Fig. 8(c)] exhibit a qualitative correspondence with the states within the jam calculated through the density definition [Figs. 8(d) and 8(e)]. The latter states are related to the speed and density found at a fixed time moment 31.5 min [Figs. 6(f) and 6(g)]. Nevertheless, there are some quantitative differences between speed and density distributions found through detector measurements [Figs. 8(b) and 8(c)] and through the use of the density definition in Figs. 8(d) and 8(e). In particular, there are points in the flow-density plane found in the density calculation through the density definition [Fig. 8(d)], which are related to greater density up to the maximum jam density. These points cannot usually be found based on traffic measurements at a detector location [Figs. 8(b) and 8(c)].

Probability densities of time headways in different traffic phases as well as in jam outflows, downstream and upstream jam fronts, which have been calculated for simulated single vehicle data discussed in Fig. 6, show that empirical conditions (2)–(4) are satisfied in numerical simulations.

B. Spontaneous emergence of moving blanks within wide moving jams in heterogeneous synchronized flow

To understand possible scenarios of emergence of moving blanks within a wide moving jam, spontaneous jam emergence in synchronized flow of a general pattern (GP) at an on-ramp bottleneck has been simulated in heterogeneous flow consisting of passenger cars and long vehicles (Fig. 9). First, an $\mathrm{F}\rightarrow\mathrm{S}$ transition occurs spontaneously at the bottleneck. Synchronized flow that appears due to this $\mathrm{F}\rightarrow\mathrm{S}$ transition propagates upstream. Moving jams emerge spontane-

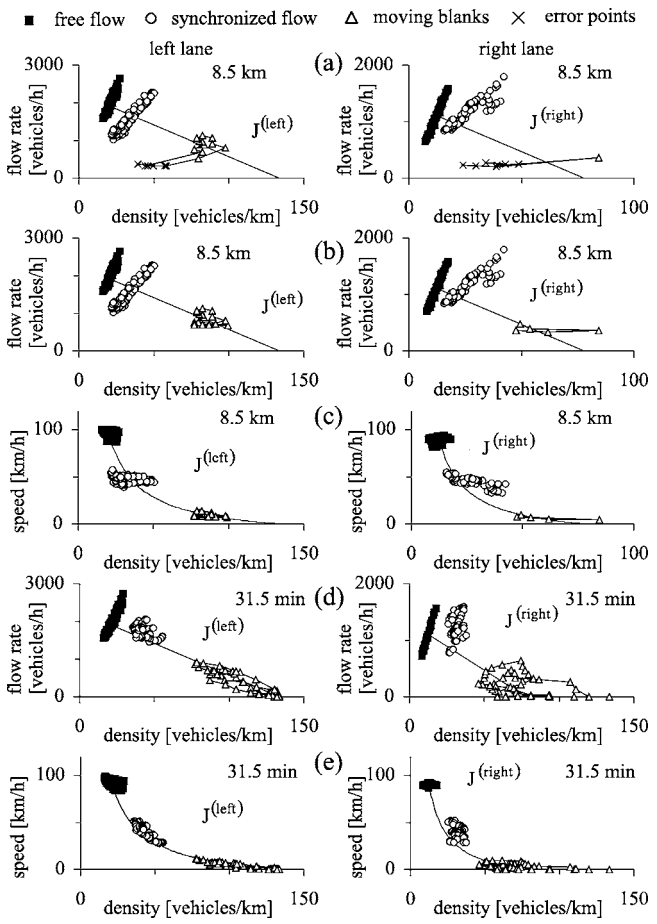

FIG. 8. Simulated characteristics of moving blanks within the wide moving jam shown in Fig. 6(a) together with states of free flow and synchronized flow in the flow-density [(a), (b), and (d)] and speed-density planes [(c) and (e)]. Left and right figures are related to the left and right lanes, respectively: (a)–(c) States within the jam that are determined at detector at $x=8.5$ km through the formula $\rho=q/v$ in two cases in which all states within the jam measured at the detector are shown (a) and error states are removed (b) and (c). (d) and (e) States within the jam that are determined through the density definition (vehicles per freeway length) at time 31.5 min. Average over five vehicles in vehicle platoons is used. $J^{(\mathrm{left})}$ and $J^{(\mathrm{right})}$ are the lines J in (a), (b), and (d) in the left and right lanes, respectively, and the associated curves J in (c) and (e) for the downstream jam front.

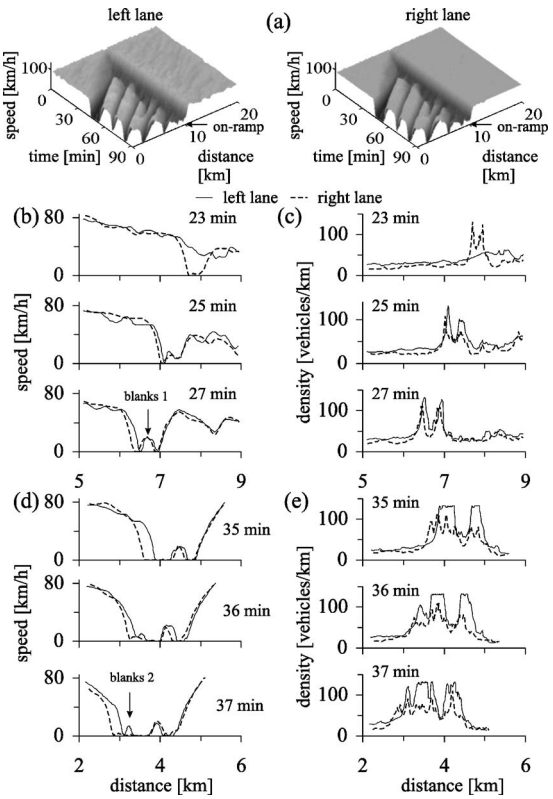

FIG. 9. Simulated characteristics of emergence of moving blanks: (a) Speed in space and time within a general pattern (GP) at an on-ramp bottleneck in the left (left) and right lanes (right). (b)–(e) Speed [(b) and (d)] and density [(c) and (e)] at different time moments associated with the GP in (a) in the left and right lanes. In (c) and (e), for density calculation the density definition (vehicles per freeway length) is used. $q_{\mathrm{in}}=1714$, $q_{\mathrm{on}}=450$ vehicles/h/lane. Model and bottleneck parameters are the same as those in Fig. 6.

ously in that synchronized flow propagating upstream.

Simulations show that there are the following mechanisms for emergence of moving blanks within the jams: (i) Vehicle lane changing at the upstream jam front. (ii) Vehicles come to a stop at the upstream front of the wide moving jam at different space gaps to the related preceding vehicles. (iii) When vehicles move with low speeds covering downstream blanks within the jam, vehicle lane changing can result in new moving blanks.

In heterogeneous flow, moving blanks emerge most frequently due to vehicle lane changing [items (i) and (iii)]. Specifically, a moving jam emerges first in the right lane only [$t=23$ min in Figs. 9(b), 9(c), and 10(a)]. Then some vehicles change from the right lane to the left lane [arrow 1 in Fig. 10(a)]. On the one hand, this lane changing decreases speed in the left lane. This leads to narrow jam formation in this lane. On the other hand, blanks between vehicles in the right lane increase due to lane changing. Vehicles begin to cover these blanks [$t\approx 24$ min in Fig. 10(a)]. As a result, low speed states within the jam appear associated with these moving blanks. Later, subsequent lane changing of vehicles from the right to the left lane results in an abrupt decrease in speed in the left lane upstream of the narrow moving jam [$t\approx 25$ min in Figs. 9(b), 9(c), and 10(a)]. Then this complex spatiotemporal speed distribution in the left lane transforms into a wide moving jam with moving blanks within the jam [$t\approx 27$ min in Figs. 9(b), 9(c), and 10(a)]. Thus, in this scenario vehicle lane changing from the right to the left lane at the upstream jam front is the main reason for emergence of moving blanks within the jam [moving blanks labeled "blanks 1" in Fig. 9(b)].

During subsequent jam propagation new moving blanks emerge [Figs. 9(d) and 9(e)]. First, the upstream jam front in the right lane is upstream of the upstream jam front in the left lane [$t=35$ min, Figs. 9(d) and 9(e)]. Due to lane changing of vehicles from the right to the left lane, the upstream jam front locations are synchronized with each other [arrow 3 in Fig. 10(b)]. This lane changing causes emergence of

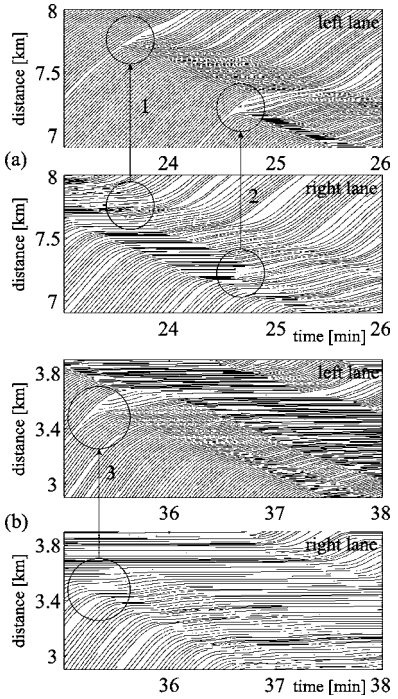

FIG. 10. Simulated characteristics of emergence of moving blanks in the GP shown in Fig. 9(a): (a) and (b) Vehicle trajectories for different time intervals in the left and right lanes.

moving blanks within the jam [$t=37$ min, moving blanks labeled "blanks 2" in Fig. 9(d)].

Note that vehicle lane changing from the right to the left lane at the upstream jam front is due to a tendency towards equalizing of the upstream jam front velocities in the left and right lanes. Indeed, long vehicles move mostly in the right lane. Therefore for the jam densities in the right $\rho_{\max}^{(\mathrm{right})}$ and left lanes $\rho_{\max}^{(\mathrm{left})}$ the condition $\rho_{\max}^{(\mathrm{right})} < \rho_{\max}^{(\mathrm{left})}$ is satisfied. Due to this condition, at flow rates $q_{\mathrm{up}}^{(\mathrm{left})}$, $q_{\mathrm{up}}^{(\mathrm{right})}$ and densities $\rho_{\mathrm{up}}^{(\mathrm{left})}$, $\rho_{\mathrm{up}}^{(\mathrm{right})}$ upstream of the jam found in simulations we would find that without lane changing the absolute value of the velocity of the upstream jam front in the left lane is smaller than the one in the right lane, as it follows from the formula

$$v_{\mathrm{up}}^{(\mathrm{lane})} = \frac{q_{\mathrm{up}}^{(\mathrm{lane})} - q_{\mathrm{jam}}^{(\mathrm{lane})}}{\rho_{\mathrm{up}}^{(\mathrm{lane})} - \rho_{\max}^{(\mathrm{lane})}}, \tag{5}$$

where the superscript "lane" means either "left" or "right" for the related lane; $q_{\mathrm{jam}}^{(\mathrm{lane})}$ is the average flow rate within the jam in the related lane. Vehicle lane changing from the right to the left lane equalizes these front velocities, as found in the numerical simulations.

C. Spontaneous emergence of wide moving jams and moving blanks in traffic with identical vehicles

Moving blanks can also emerge spontaneously within a wide moving jam that appears in freeway traffic with identical vehicles. We consider wide moving jams, which emerge within dissolving GPs (DGP) shown in Figs. 11(a) and 11(b) (see explanations of DGP emergence in Sec. IV A).

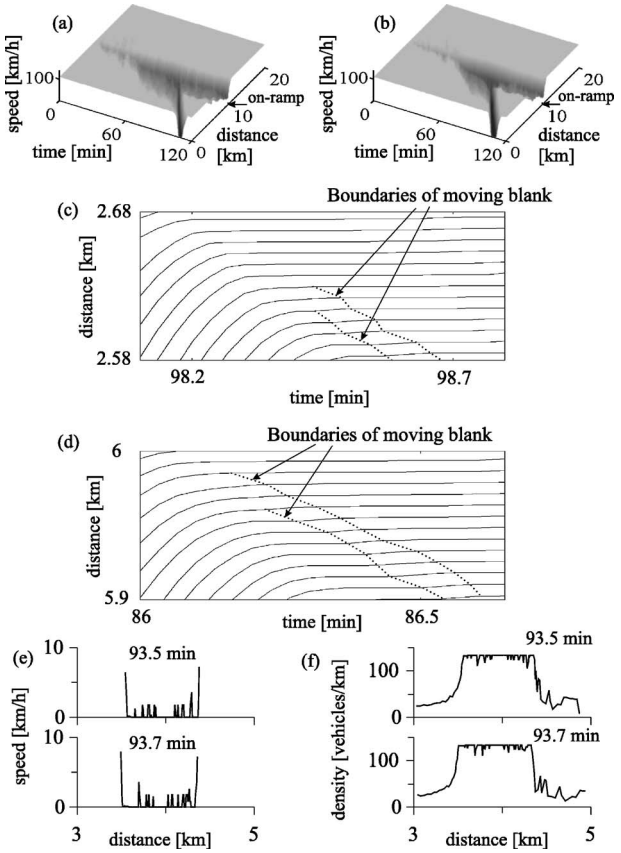

FIG. 11. Simulated characteristics of emergence of moving blanks within wide moving jams in dissolving GPs (DGP): (a) and (b) Speed in space and time within DGPs at on-ramp bottleneck on a two-lane road (a) and on a single-lane road (b). (c) and (d) Vehicle trajectories within the jam for the DGP in (a) and for the DGP in (b), respectively. (e) and (f) Spatial distributions of speed (e) and density (f) for the DGP in (b) for two time moments. In (f), for density calculation the density definition (vehicles per freeway length) is used. Stochastic three-phase traffic model of identical vehicles (Sec. 16.3 of Ref. [1]). $q_{\mathrm{in}}=1946$ vehicles/h/lane. $q_{\mathrm{on}}=240$ (a) and 345 vehicles/h/lane (b). $x_{\mathrm{on}}=10$ km, $L_{\mathrm{m}}=300$ m. In (a) and (c), data for the left lane is shown.

Simulations show that in the case of a two-lane main road [Fig. 11(a)] there are the same three mechanisms for moving blank emergence within the jams as those in heterogeneous flow [items (i)-(iii) of Sec. III B]. However, in contrast with heterogeneous flow, in traffic with identical vehicles the mechanism of emergence of moving blanks associated with vehicle lane changing at the upstream jam front [item (i)] is a rare event: In traffic with identical vehicles, velocities of upstream jam fronts in different lanes are approximately equal to each other.

Simulations show that moving blanks in traffic with identical vehicles occur most frequently due to the mechanism of item (ii) [Fig. 11(c)]. This mechanism is the only possible one for emergence of moving blanks in the case of a single-lane road [Figs. 11(b) and 11(d)]. As a result, on the single-lane road the quantity of the moving blanks is the smallest one [Figs. 11(d)–11(f)] in comparison with moving blanks within wide moving jams that emerge on the two-lane road

and in heterogeneous flow. Note that boundaries of a moving blank within the jam can be complex space and time functions [Figs. 11(c) and 11(d)].

IV. MICROSCOPIC EFFECTS OF MOVING JAM EMERGENCE, PROPAGATION, AND DISSOLUTION

A. Diverse transitions between traffic phases and states

Microscopic effects of moving jam emergence, propagation, and dissolution lead to diverse *transitions* between traffic phases and traffic states. In a microscopic analysis of these transitions, we should distinguish the following three basic types of qualitatively different transitions measured at fixed freeway locations. (i) Local phase transitions (denoted by $F \rightarrow S$, $S \rightarrow F$, $S \rightarrow J$, and $J \rightarrow S$ transitions): Within a local freeway region a new traffic phase emerges instead of an initial traffic phase. (ii) Transitions between existing traffic phases that are caused by propagation of a front separating free and synchronized flows or by wide moving jam propagation. (iii) Transitions between different traffic states of the same traffic phase. We consider the associated microscopic effects on an example of moving jam emergence within the DGP shown in Fig. 11(b).

First, an $F \rightarrow S$ transition occurs in a neighborhood of the bottleneck [location $x=10.4$ km; transition of type (i) shown by arrows labeled "$F \rightarrow S$" in Figs. 12(a) and 12(b)]. As a result, synchronized flow appears at the bottleneck. Second, this synchronized flow propagates on the main road upstream of the bottleneck, i.e., a wave of upstream transitions from free flow to synchronized flow occurs [e.g., $x=9.1$, 7.4, and 5.5 km; transitions of type (ii) shown by arrows 1–3 in Figs. 12(c)–12(h)]. Then a self-compression of this synchronized flow (pinch effect) within a localized region upstream of the bottleneck occurs. The pinch effect causes an abrupt transition between different states within the synchronized flow phase [$x=9.1$ km; transition of type (iii) shown by arrows labeled "P" in Figs. 12(c) and 12(d)].

Within the related pinch region of synchronized flow, a narrow moving jam emerges spontaneously. During upstream jam propagation, the jam amplitude grows and the narrow moving jam transforms into a wide moving jam, i.e., an $S \rightarrow J$ transition occurs in the synchronized flow [location $x=7.4$ km; transition of type (i) shown by arrows labeled "$S \rightarrow J$" in Figs. 12(e) and 12(f)]. The flow rate in the jam outflow q_{out} is smaller than the flow rate in the pinch region. As a result, the pinch region dissolves after the wide moving jam has been formed; synchronized flow of higher speed remains [$x=9.1$ km; transition of type (iii) shown by arrows labeled "S" in Figs. 12(c) and 12(d)]. For this reason, in contrast with the GP in Fig. 9(a) the wide moving jam in Fig. 11(b) prevents subsequent moving jam emergence in synchronized flow upstream of the bottleneck, i.e., the DGP appears [54].

The resulting DGP consists of synchronized flow upstream of the wide moving jam, the jam propagating upstream, and synchronized flow that is downstream of the jam and upstream of the bottleneck [Fig. 11(b)]. At each of the virtual detectors, jam propagation causes different transitions of type (ii): (1) From an initial traffic phase at a detector (free flow or synchronized flow) to low speed states associated with moving blanks within the wide moving jam [e.g., $x=5.5$ km, transition from synchronized flow to the jam shown by arrows "4" in Figs. 12(g) and 12(h)]. (2) From the jam to either free flow or synchronized flow after the jam has passed the detector [$x=7.4$ km, transition from the jam to synchronized flow shown by arrows "5" in Figs. 12(e) and 12(f) and $x=5.5$ km, transition from the jam to free flow shown by arrows "6" in Figs. 12(g) and 12(h)].

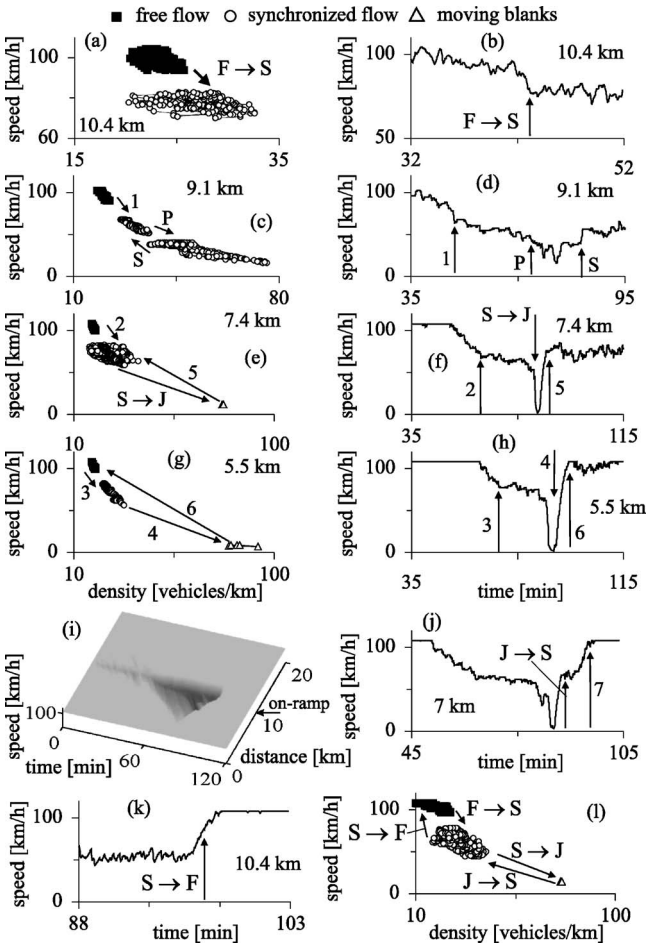

FIG. 12. Simulated characteristics of microscopic transitions between different traffic phases and states measured at fixed freeway locations as well as the associated hysteresis phenomena in traffic flow: (a)–(h) Transitions in the speed-density plane [(a), (c), (e), and (g)] and in the related time-dependences of speed [(b), (d), (f), and (h)] at different road locations during wide moving jam emergence and propagation shown in Fig. 11(b). (i)–(k) Speed in time and space during a dissolution of the DGP in Fig. 11(b) occurring when q_{in} decreases to 900 vehicles/h at $t=75$ min (i) and the associated transitions in time-dependences of speed [(j) and (k)] at different road locations. (l) States of the three traffic phases associated with double Z-characteristic in the speed-density plane for local phase transitions. Time-dependences of speed are single vehicle data. $q_{out}=1810$ vehicles/h. For data in the speed-density plane, moving averaging over five vehicles is used.

In Figs. 11(b) and 12(a)–12(h), the flow rates q_{on} and q_{in} do not vary over time. In contrast, if q_{in} begins to decrease, then the DGP dissolves [Fig. 12(i)]. In this case, DGP dissolution starts upstream and propagates downstream [55]. First,

a wave of synchronized flow dissolution, which is upstream of the jam, propagates downstream leading to transitions of type (ii) from synchronized flow to free flow [Fig. 12(i)]. When this wave reaches the jam, the latter begins to dissolve. As a result of wide moving jam dissolution synchronized flow remains, i.e., an J→S transition occurs [$x=7$ km; arrows labeled "J→S" in Figs. 12(j) and 12(l)]. Then a new wave of synchronized flow dissolution propagating downstream is formed, which leads to transitions of type (ii) from synchronized flow to free flow [$x=7$ km; arrow 7 in Fig. 12(j)]. Due to the latter transitions, finally, an S→F transition [transition of type (i)] occurs at the bottleneck [$x=10.4$ km; arrows labeled "S→F" in Figs. 12(k) and 12(l)].

These numerical simulations enable us to find states of free flow and synchronized flow as well as states within a wide moving jam on a double Z-characteristic for phase transitions [1] [Fig. 12(l)]. Arrows between these states labeled "F→S" and "S→F" are associated with F→S and S→F transitions at the bottleneck ($x=10.4$ km), whereas arrows labeled "S→J" and "J→S" are associated with S→J and J→S transitions, which have occurred at different locations, $x=7.4$ and 7 km, respectively [Figs. 12(f) and 12(j)]. Thus wide moving jam emergence (S→J transition) and dissolution (J→S transition) occur upstream of the bottleneck, whereas the F→S and S→F transitions occur at the bottleneck. As a result, all of these phase transitions between states for the three traffic phases on the double Z-characteristic cannot be found through measurements of traffic variables at a single freeway location. Consequently, traffic states and transitions shown by arrows in Fig. 12(l) are taken from different locations [i.e., from Figs. 12(a), 12(b), 12(e), 12(f), 12(j), and 12(k)] at which the related local phase transitions have occurred.

We can conclude that during synchronized flow and wide moving jam emergence, propagation, and dissolution there are all three types of abrupt transitions (i), (ii), and (iii) between traffic variables. These transitions can cause a variety of "hysteresis" phenomena in the speed-density plane [Figs. 12(c), 12(e), 12(g), and 12(l)]. Specifically, we find transitions of type (i) caused by local first-order phase transitions between the free flow, synchronized flow, and wide moving jam traffic phases [arrows labeled "F→S," "S→F," "S→J," and "J→S" in Figs. 12(a), 12(b), 12(e), 12(f), and 12(j)–12(l)]. Transitions of type (ii) caused by upstream (arrows 1–3 in Fig. 12) or downstream (arrow 7) propagation of the front between free and synchronized flows, or else upstream wide moving jam propagation (arrows 4–6). Transitions of type (iii) caused by pinch region emergence [arrows *P* in Figs. 12(c) and 12(d)] and pinch region dissolution in synchronized flow (arrows *S*).

B. Jam propagation loops: Nature of Treiterer's hysteresis phenomenon

If traffic variables are measured along a vehicle platoon going through the wide moving jam of the DGP shown in Fig. 11(b), then abrupt transitions between traffic variables in the flow-density and speed-density planes exhibit peculiarities (Fig. 13) in comparison with measurements at virtual detectors presented in Fig. 12.

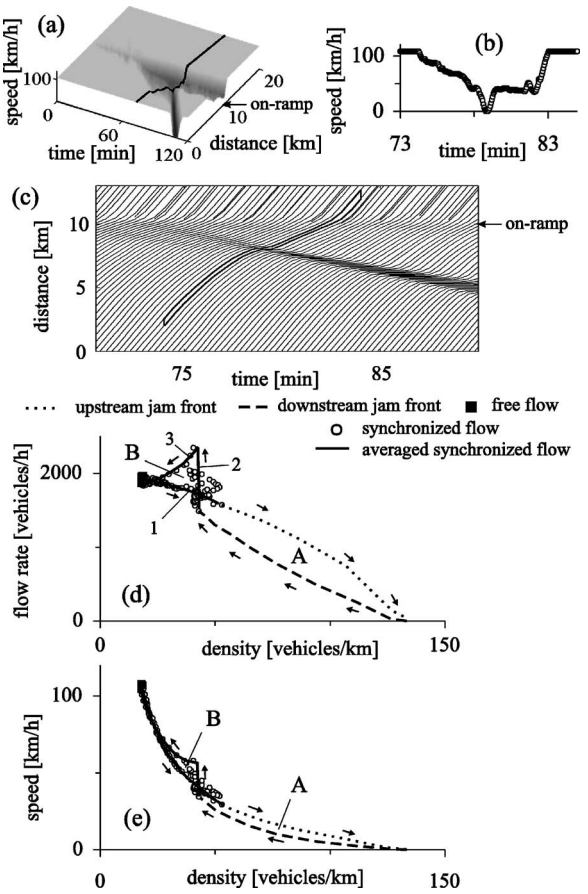

FIG. 13. Simulated characteristics of microscopic features of moving jam propagation: (a) Speed in time and space in the DGP taken from Fig. 11(b) with average trajectory (solid curve) associated with a platoon of seven vehicles going through the DGP. (b) Average speed within the platoon propagating through the wide moving jam and synchronized flow phases formed in the DGP. (c) Vehicle trajectories within the DGP in which the vehicle platoon related to (b) is marked by a solid block. (d) and (e) Flow-density (d) and speed-density relationships (e) associated with the platoon of seven vehicles going through the wide moving jam and synchronized flow phases related to the DGP in (a)–(c). Other parameters are as those in Fig. 11(b). In (c), trajectories of each tenth vehicle are shown.

A platoon of seven vehicles is considered that is going through the moving jam and other traffic states related to the DGP [Figs. 13(a)–13(c)]. Within the platoon the density ρ is calculated at each given time moment, i.e., in accordance with the density definition (vehicles per freeway length). The flow rate associated with the platoon is $q=\rho v$, where v is average vehicle speed within the platoon. It turns out that traffic states in the flow-density and speed-density planes associated with speed and density within the platoon exhibit two loops labeled *A* and *B* in Figs. 13(d) and 13(e). The loops are associated with different characteristics of the three traffic phases passing by the vehicle platoon going through the DGP [solid curve in Fig. 13(a)]. These numerical results [Figs. 13(d) and 13(e)] explain empirical results of Treiterer

et al. [18,19] found in their study of vehicle trajectories within a moving jam, which emerged and propagated upstream of an on-ramp bottleneck.

To understand these statements, note that the chosen vehicle platoon [solid curve in Fig. 13(a)] is going first through free flow [$t<74$ min in Figs. 13(a) and 13(b)]. Second, the platoon must decelerate when it reaches synchronized flow, which is upstream of the wide moving jam. In this synchronized flow, speed decreases during the platoon propagation [$74<t<78$ min in Figs. 13(a) and 13(b)]. The associated synchronized flow states lie at lower speed and greater density in the flow-density and speed-density planes than the speed and density within the platoon in free flow, respectively [curve 1 in Fig. 13(d)]. Third, the platoon meets the upstream jam front within which the vehicles must decelerate to the speed within the jam [this speed is almost as low as zero; $t\approx78.5$ min in Figs. 13(a) and 13(b)]. Consequently, the flow rate and speed sharply decrease and density increases [curves for the upstream jam front in Figs. 13(d) and 13(e)]. Later, due to upstream jam propagation the vehicles within the platoon can accelerate at the downstream jam front [$t\approx79$ min in Figs. 13(a) and 13(b)]. As a result, the flow rate and speed sharply increase and density decreases [curves for the downstream jam front in Figs. 13(d) and 13(e)]. We see that at the upstream jam front the density is greater than at the downstream front at the same speed: As in empirical results of Sec. II D, in the simulations vehicles decelerating at the upstream jam front accept shorter time headways than time headways of vehicles accelerating at the downstream jam front.

Then the platoon moves through synchronized flow downstream of the jam. In this synchronized flow, the speed is lower than in free flow upstream of the jam and downstream of the bottleneck [$79.5<t<82$ min in Figs. 13(a) and 13(b)]. This platoon propagation is also associated with the synchronized flow within the merging region of the on-ramp bottleneck [Figs. 13(a)–13(c)]. Within this region due to vehicle merging from the on-ramp onto the main road time headways within the platoon decrease. Therefore the flow rate is a sharply increasing function of freeway location. For this reason, traffic states in the flow-density and speed-density planes associated with the platoon, which is going through synchronized flow downstream of the jam, exhibit rapid flow rate growth with a slightly increasing speed. These synchronized flow states lie at lower speed and greater density in the flow-density and speed-density planes than the speed and density in free flow, respectively [curve 2 in Fig. 13(d)]. This growth of the flow rate results in the loop labeled *A* in the flow-density and speed-density planes. This loop is formed by the upstream and downstream jam fronts together with a part of the curve 2 related to the synchronized flow downstream of the jam [Figs. 13(d) and 13(e)].

Later, the platoon propagates through the downstream front of synchronized flow in which the speed increases considerably to the speed in free flow downstream of the bottleneck [$t\approx82.5$ min in Fig. 13(b)]. Hence traffic states related to the platoon propagating through the downstream front of synchronized flow at the bottleneck exhibit rapid speed growth in the flow-density and speed-density planes [curve 3 in Fig. 13(d)]. Consequently, the platoon propagation through synchronized flow upstream of the jam (curve 1), through synchronized flow downstream of the jam (curve 2), as well as through the downstream front of the synchronized flow at the bottleneck up to free flow downstream of this front (curve 3) leads to the second loop labeled *B* in the flow-density and speed-density planes [Figs. 13(d) and 13(e)].

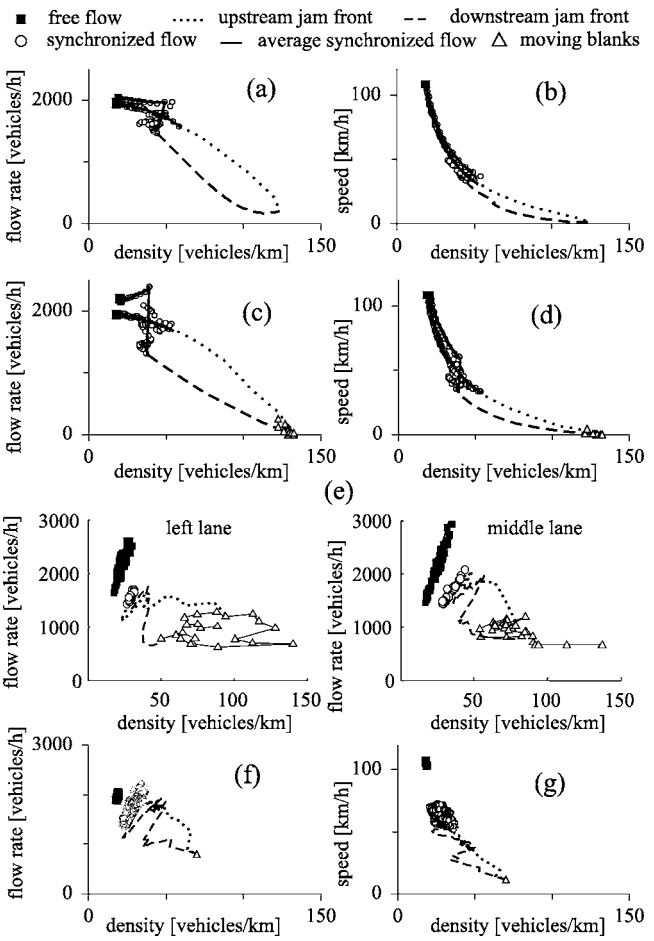

FIG. 14. Simulated [(a)–(d), (f), and (g)] and empirical (e) jam propagation loops: (a)–(d) Flow-density [(a) and (c)] and speed-density relationships [(b) and (d)] of two different platoons of seven vehicles going through the wide moving jam and other traffic phases within the DGP shown in Fig. 13(a). Platoons in (a) and (b) and (c) and (d) are going through the DGP, respectively, earlier and later than the platoon in Fig. 13(a). (e) Empirical flow-density relationships in the left (figure left) and middle (figure right) lanes associated with the wide moving jam in Figs. 2(a)–2(h). (f) and (g) Simulated flow-density (f) and speed-density relationships (g) associated with moving averaging of speed v and flow rate q within platoons of seven vehicles going through a virtual detector at $x=8$ km within the DGP shown in Fig. 13(a).

Simulations show that loops' shapes depend on the chosen vehicle platoon. If a platoon of seven vehicles is chosen, which propagates earlier through the DGP than the platoon considered in Figs. 13(b)–13(e), then the loops *A* and *B* [Figs. 14(a) and 14(b)] are different from those in Figs. 13(d) and 13(e). There are several reasons for this result. First, free flow and synchronized flow states within the platoon upstream and downstream of the jam depend on the chosen

platoon considerably. Second, in Figs. 14(a) and 14(b) the platoon is going through a narrow moving jam rather than through a wide moving one.

If another platoon of seven vehicles is chosen, which propagates later through the DGP than the platoon considered in Figs. 13(b)–13(e), then the shape of the loops *A* and *B* [Figs. 14(c) and 14(d)] is different from those in Figs. 13(d), 13(e), 14(a), and 14(b). The first reason for this different behavior is the same as that mentioned above. In addition, in this case the platoon is going through a wide moving jam whose width is greater than the width of the wide moving jam associated with the platoon chosen in Figs. 13(b)–13(e). As a result, there are low speed states within the jam associated with moving blanks within the jam.

In general, average space gaps and speeds within a platoon depend on the time interval, when the platoon is going through a moving jam, through synchronized flows and free flows upstream and downstream of the jam. This can change both loops *A* and *B* in Figs. 14(a) and 14(c) associated with a vehicle platoon going through the DGP appreciably. Moreover, the flow rate in free flow downstream of the bottleneck associated with a vehicle platoon can be very different for different platoons. This is due to considerable variations in space gaps between vehicles within different platoons after the platoons have passed the downstream front of synchronized flow at the bottleneck. This explains different flow rates in the free flow associated with three vehicles platoons in Figs. 13(d), 13(e), and 14(a)–14(d). Apparently, this complex loop behavior can explain very different loops *A* and *B* observed in the empirical study by Treiterer *et al.* [18,19].

The loops in the flow-density and speed-density planes shown in Figs. 13(d), 13(e), and 14(a)–14(d) are associated with measurements of the density within the vehicle platoon in accordance with the density definition (vehicles per freeway length). The use of the density definition is possible if vehicle trajectories are known as this is the case in simulations presented in Figs. 13 and 14(a)–14(d) as well as in Treiterer's empirical observations of vehicle trajectories [18,19].

Unfortunately, the use of this correct procedure is not possible to perform when single vehicle data is measured by a local detector on a road as this is the case for the wide moving jam shown in Figs. 2(a)–2(g). In this case, the density has to be estimated through the formula $\rho=q/v$, in which the flow rate q and speed v are associated with time averaging over many *different* vehicle platoons passing the detector. There are two systematic errors in this case: (i) Density estimation at lower speeds within the jam [see explanations of Fig. 6(e) in Sec. III]. (ii) Because of fluctuations, measured and estimated traffic variables associated with different platoons passing the detector do not coincide with the respective traffic variables found for a single platoon going through the wide moving jam and other traffic phases in Fig. 13.

Apparently, these errors lead to qualitative different empirical loops in the flow-density plane [Fig. 14(e)] for the jam shown in Figs. 2(a)–2(g) in comparison with empirical observations by Treiterer *et al.* [18,19]. These conclusions are confirmed by numerical simulations in which the same procedure of the density estimation through detector measurements is used [Figs. 14(f) and 14(g)] as that in empirical Fig. 14(e). The simulated loops in the flow-density and speed-density planes [Figs. 14(f) and 14(g)] associated with traffic variables determined at a detector location within the DGP shown in Fig. 13(a) are qualitatively different from the loops found through the use of the correct density calculation associated with vehicle platoon propagation through the DGP [Figs. 13(d) and 13(e)].

V. DISCUSSION

Based on empirical and simulated results presented, the following conclusions can be made:

(i) Between the upstream and downstream wide moving jam fronts there is a complex microscopic spatiotemporal structure, which consists of alternations of regions in which traffic flow is interrupted and flow states of low speeds associated with moving blanks within the jam. Moving blanks within a wide moving jam resemble electron holes in the valence band of semiconductors: As the moving blanks that propagate upstream appear due to downstream vehicle motion within the jam, so appearance of electron holes moving with the electric field results from electron motion against the electric field in the valence band of semiconductors.

(ii) Moving blanks exhibit a nonregular spatiotemporal behavior. The moving blanks are often not synchronized between different freeway lanes.

(iii) Lane changing at the upstream front of a wide moving jam can lead to wide (in the longitudinal direction) moving blanks within the jam.

(iv) Moving blanks emergence is characterized by random changes of the upstream jam front location in some of the freeway lanes over time.

(v) The mean time headway for moving blanks is longer than the one for synchronized flow. The mean time headway for downstream jam fronts is longer than mean time headways for jam outflows and upstream jam fronts. There is a difference between the mean time headway for jam outflows and the mean time delay in driver acceleration at the downstream jam front. This difference is proportional to the mean space gap between vehicles stopped within wide moving jams.

(vi) To find correct traffic characteristics measured at fixed freeway locations, measurement points, which are related to the flow interruption effect within wide moving jams and lead to a large systematic error in density estimation, have to be removed.

(vii) Microscopic effects of synchronized flow and moving jam emergence, propagation, and dissolution lead to diverse transitions between the three traffic phases as well as different traffic states of the same traffic phase. These transitions are responsible for a variety of hysteresis phenomena in traffic flow. The physics of a particular hysteresis phenomenon can only be adequately understood if *spatiotemporal* congested pattern features associated with the phenomenon are known.

(viii) In simulations, there are two loops in the flow-density plane associated with a vehicle platoon propagation through a moving jam as well as through free flow and synchronized flow states of traffic upstream and downstream of

the jam. The loops are associated with different characteristics of the three traffic phases, free flow, synchronized flow, and wide moving jam passing by the platoon. These simulation results made in the context of three-phase traffic theory disclose the nature of an empirical hysteresis phenomenon in traffic flow found by Treiterer *et al.* [18,19].

APPENDIX: MEAN TIME HEADWAY IN JAM OUTFLOW

To explain Eq. (4), we use the formula for the outflow jam rate [1]

$$q_{\text{out}}^{(\text{syn})} = (1 - \rho_{\text{min J}}^{(\text{syn})}/\rho_{\max})/\tau_{\text{del}}^{(\text{ac})}. \tag{A1}$$

Using the relation $\rho_{\text{min J}}^{(\text{syn})} = q_{\text{out}}^{(\text{syn})}/v_{\text{max J}}^{(\text{syn})}$, from Eq. (A1) we get

$$(q_{\text{out}}^{(\text{syn})})^{-1} = \tau_{\text{del}}^{(\text{ac})} + (v_{\text{maxJ}}^{(\text{syn})}\rho_{\max})^{-1}. \tag{A2}$$

When free flow is formed in a jam outflow, $v_{\text{max J}}^{(\text{syn})} = v_{\max}$, $q_{\text{out}}^{(\text{syn})} = q_{\text{out}}$, and $\rho_{\text{min J}}^{(\text{syn})} = \rho_{\min}$ [1].

When $q_{\text{out}}^{(\text{syn})}$ is measured at a detector, $q_{\text{out}}^{(\text{syn})} = N/T$, where N is the number of vehicles passing the detector during time T, which is equal to the sum of gross time headways $\tau_{i,i+1}^{(\text{gross})}$ of these vehicles:

$$T = \sum \tau_{i,i+1}^{(\text{gross})} = \sum (\tau_{i,i+1} + d_i/v_i). \tag{A3}$$

Then $(q_{\text{out}}^{(\text{syn})})^{-1}$ can be written as

$$(q_{\text{out}}^{(\text{syn})})^{-1} = N^{-1} \sum (\tau_{i,i+1} + d_i/v_i). \tag{A4}$$

Assuming that there is no correlation between vehicle length and speed, we obtain an approximate formula

$$(q_{\text{out}}^{(\text{syn})})^{-1} = \bar{\tau}_{\text{out}}^{(\text{syn})} + \bar{d}\overline{v^{-1}}, \tag{A5}$$

$\overline{v^{-1}} = N^{-1}\Sigma(1/v_i)$. From a comparison of Eqs. (A2) and (A5), we obtain

$$\bar{\tau}_{\text{out}}^{(\text{syn})} = \tau_{\text{del}}^{(\text{ac})} + \bar{d}_{\text{jam}}(v_{\text{maxJ}}^{(\text{syn})})^{-1} - \bar{d}\overline{v^{-1}}. \tag{A6}$$

If $\overline{v^{-1}} \approx (v_{\text{max J}}^{(\text{syn})})^{-1}$, from Eq. (A6) we get formula (4).

[1] B. S. Kerner, *The Physics of Traffic* (Springer, Berlin, 2004).
[2] *Special Report 165: Revised Monograph on Traffic Flow Theory*, edited by N. H. Gartner, C. J. Messer, and A. Rathi (Transportation Research Board, Washington, D.C., 1997).
[3] D. E. Wolf, Physica A **263**, 438 (1999).
[4] D. Chowdhury, L. Santen, and A. Schadschneider, Phys. Rep. **329**, 199 (2000).
[5] D. Helbing, Rev. Mod. Phys. **73**, 1067 (2001).
[6] T. Nagatani, Rep. Prog. Phys. **65**, 1331 (2002).
[7] K. Nagel, P. Wagner, and R. Woesler, Oper. Res. **51**, 681 (2003).
[8] R. Mahnke, J. Kaupužs, and I. Lubashevsky, Phys. Rep. **408**, 1 (2005).
[9] *Transportation and Traffic Theory*, *Proceedings of the 16th International Symposium on Transportation and Traffic Theory*, edited by H. S. Mahmassani (Elsevier, Amsterdam 2005).
[10] *Traffic and Granular Flow' 99*, edited by D. Helbing, H. J. Herrmann, M. Schreckenberg, and D. E. Wolf (Springer, Heidelberg 2000).
[11] *Traffic and Granular Flow' 01*, edited by M. Fukui, Y. Sugiyama, M. Schreckenberg, and D. E. Wolf (Springer, Heidelberg 2003).
[12] *Traffic and Granular Flow' 03*, edited by S. P. Hoogendoorn, S. Luding, P. H. L. Bovy, M. Schreckenberg, and D. E. Wolf (Springer, Heidelberg 2005).
[13] A. S. Mikhailov, *Foundations of Synergetics Vol. I*, 2nd ed. (Springer, Berlin 1994).
[14] B. S. Kerner and V. V. Osipov, *Autosolitons: A New Approach to Problems of Self-Organization and Turbulence* (Kluwer, Dordrecht, 1994).
[15] L. C. Edie and R. S. Foote, Highw. Res. Board, Proc. Annu. Meet. **37**, 334 (1958).
[16] L. C. Edie and R. S. Foote, in *Highway Research Board Proceedings* 39, (HRB, National Research Council, Washington, D.C. 1960), pp. 492–505.
[17] L. C. Edie, Oper. Res. **9**, 66 (1961).
[18] J. Treiterer and J. A. Myers, in *Proceedings of the 6th International Symposium on Transportation and Traffic Theory*, edited by D. J. Buckley (A. H. & A. W. Reed, London, 1974), pp. 13–38.
[19] J. Treiterer, Ohio State University Technical Report PB 246 094, Columbus, Ohio, 1975.
[20] M. Koshi, M. Iwasaki, and I. Ohkura, in *Proceedings of the 8th International Symposium on Transportation and Traffic Theory*, edited by V. F. Hurdle *et al.* (University of Toronto Press, Toronto, Ontario 1983) p. 403.
[21] B. S. Kerner and P. Konhäuser, Phys. Rev. E **50**, 54 (1994).
[22] B. S. Kerner, P. Konhäuser, and M. Schilke, Phys. Rev. E **51**, R6243 (1995).
[23] D. Helbing, A. Hennecke, and M. Treiber, Phys. Rev. Lett. **82**, 4360 (1999).
[24] H. Y. Lee, H.-W. Lee, and D. Kim, Phys. Rev. E **59**, 5101 (1999).
[25] M. Treiber, A. Hennecke, and D. Helbing, Phys. Rev. E **62**, 1805 (2000).
[26] B. S. Kerner, Phys. Rev. Lett. **81**, 3797 (1998).
[27] B. S. Kerner, Phys. Rev. E **65**, 046138 (2002).
[28] It should be noted that in contrast to *spontaneous* moving jam emergence, which is not observed in free flow, induced moving jam emergence in free flow can seldom be observed in real freeway traffic. This occurs, for example, if first a moving jam emerges spontaneously in *synchronized* flow within an off-ramp lane. Then due to upstream jam propagation in the off-ramp lane, the jam can reach the main road in which currently free flow is realized. If this free flow is in a metastable state with respect to wide moving jam formation, the jam grows and transforms into a wide moving jam on the main road (see an empirical example of such induced wide moving jam emergence in free flow in Sec. 12.6 of [1]).

[29] B. S. Kerner and S. L. Klenov, J. Phys. A **35**, L31 (2002).
[30] B. S. Kerner, S. L. Klenov, and D. E. Wolf, J. Phys. A **35**, 9971 (2002).
[31] B. S. Kerner and S. L. Klenov, e-print physics/0507120; J. Phys. A **39**, 1775 (2006).
[32] B. S. Kerner and S. L. Klenov, Phys. Rev. E **68**, 036130 (2003).
[33] B. S. Kerner and S. L. Klenov, J. Phys. A **37**, 8753 (2004).
[34] B. S. Kerner, S. L. Klenov, and A. Hiller, e-print physics/0507094; J. Phys. A **39**, 2001 (2006).
[35] L. Neubert, L. Santen, A. Schadschneider, and M. Schreckenberg, Phys. Rev. E **60**, 6480 (1999).
[36] W. Knospe, L. Santen, A. Schadschneider, and M. Schreckenberg, Phys. Rev. E **65**, 056133 (2002).
[37] W. Knospe, L. Santen, A. Schadschneider, and M. Schreckenberg, Phys. Rev. E **70**, 016115 (2004).
[38] R. J. Cowan, Transp. Res. **9**, 371 (1976).
[39] T. Luttinen, Transp. Res. Rec. **1365**, 92 (1992).
[40] *Motorway Analysis: New Methodologies and Recent Empirical Findings*, edited by P. H. L. Bovy (Delft University Press, Delft 1998).
[41] B. Tilch and D. Helbing, in [10], p. 333.
[42] J. Banks, Trans. Rec. B **37**, 539 (2004).
[43] G. S. Gurusinghe, T. Nakatsuji, Y. Azuta, P. Ranjitkar, and Y. Tanaboriboon, in *Preprints of the 82nd TRB Annual Meeting*, TRB Paper No.: 03-4137 (TRB, Washington, D.C., 2003).
[44] Sometimes for better statistical conclusions, single vehicle data measured on various days or/and many different locations are aggregated to an aggregated data set. This aggregated database is further used for calculation of traffic flow characteristics.
[45] J. Kienzle, Diploma Thesis, Universität Stuttgart, Institut für Straßen-und Verkehrswesen, Stuttgart, 2001.
[46] For data shown in Fig. 1(b), from a comparison of a local traffic dynamics measured at different detectors, we find that the moving jams propagate upstream with the mean velocity of the downstream jam fronts $v_g \approx -15.5$ km/h. For data shown in Fig. 1(d), a comparison of local traffic dynamics measured at D2 (not shown) and D1 enables us to conclude that $v_g \approx -15.8$ km/h.
[47] B. S. Kerner, S. L. Klenov, A. Hiller, and H. Rehborn, e-print physics/0510167.
[48] In common speech, the term "stop-and-go" traffic is used in context with intervals of low or zero speed in traffic flow. However, this is not necessarily equivalent to flow interruption within a wide moving jam [34]. For a driver a sequence of narrow moving jams can also be considered "stop-and-go" traffic. This is because within a narrow moving jam during a short time interval $\Delta t \sim \tau_{del}^{(ac)}$ the driver can be stopped. However, the sequence of narrow moving jams is associated with the synchronized flow phase, rather than with the wide moving jam phase. Moreover, "stop-and-go" traffic can be associated with qualitatively different complex spatiotemporal sequences of various traffic phases and states. For example, "stop-and-go" traffic can be (i) a sequence of the wide moving jam and free flow phases, (ii) a sequence of the wide moving jam, free flow, and synchronized flow phases, (iii) a sequence of the free flow and synchronized flow phases, if there are narrow moving jams in the synchronized flow, or (iv) synchronized flow containing narrow moving jams. For this reason, the term "stop-and-go" traffic is not used in three-phase traffic theory [1].
[49] In Eq. (4), $\tau_{del}^{(ac)}$ has been estimated through the use of the formula $\tau_{del}^{(ac)} = 1/(|v_g|\rho_{max})$, where v_g is the mean velocity of downstream jam fronts [46]. To estimate ρ_{max}, the empirical line J in the flow-density plane has been estimated [1,50,51]. The left coordinates of the line J are $(\rho_{min\,J}^{(syn)}, q_{out}^{(syn)})$ and its slope is equal to v_g. The mean density $\rho_{min\,J}^{(syn)}$ in jam outflows is calculated through the formula $\rho_{min\,J}^{(syn)} = q_{out}^{(syn)}/v_{max\,J}^{(syn)}$, where $q_{out}^{(syn)}$ is the measured jam outflow rate. Then ρ_{max} is related to the intersection point of the line J with the density axis. When free flow is formed in a jam outflow, $v_{max\,J}^{(syn)} = v_{max}$, $q_{out}^{(syn)} = q_{out}$, and $\rho_{min\,J}^{(syn)} = \rho_{min}$ [1]. Results of these estimations are $q_{out} = 1950$ vehicle/h, $\rho_{min} = 21$ vehicles/km, $\rho_{max} = 145$ vehicles/km, and $\tau_{del}^{(ac)} = 1.58$ s for aggregated data in Fig. 2(i). $q_{out}^{(syn)} = 2040$ vehicle/h, $\rho_{min}^{(syn)} = 24.5$ vehicles/km, $\rho_{max} = 154$ vehicles/km, and $\tau_{del}^{(ac)} = 1.48$ s for data in Fig. 1(d).
[50] B. S. Kerner and H. Rehborn, Phys. Rev. E **53**, R1297 (1996).
[51] B. S. Kerner and H. Rehborn, Phys. Rev. E **53**, R4275 (1996).
[52] A detailed consideration of the models, their physics, and parameters can be found in Secs. 16.3 and 20.2 of [1]. When some other model parameters are used, they are given in figure captions.
[53] Longer time headways for moving blanks in the right lane [Fig. 6(d), right] are related to long vehicles.
[54] The flow rate q_{on} is smaller, whereas q_{in} is greater than these flow rates are in Fig. 9(a) at which the GP emerges at the bottleneck. This explains pinch region dissolution and DGP emergence.
[55] Another case has been considered in [32] in which due to a decrease in q_{on} over time a wave of congested pattern dissolution starts at the bottleneck and propagates upstream.